HHS Public Access

Author manuscript

Cell Rep. Author manuscript; available in PMC 2023 June 01.

Published in final edited form as:

Cell Rep. 2022 December 20; 41(12): 111863. doi:10.1016/j.celrep.2022.111863.

Niche-mediated repair of airways is directed in an occupant-dependent manner

Handeng Lyu[1,2,3,4], **Rachel Warren**[2,4], **Shan Gao**[2], **Kylie Klinkhammer**[2,3], **Tingting Yuan**[3], **Jin-San Zhang**[1], **Douglas Brownfield**[2], **Xiaokun Li**[1,*], **Stijn P. De Langhe**[2,3,5,*]

[1]School of Pharmaceutical Sciences, and The First Affiliated Hospital of Wenzhou Medical University, Wenzhou, Zhejiang 325000, China

[2]Department of Medicine, Division of Pulmonary and Critical Medicine, Mayo Clinic, Rochester, MN 55905, USA

[3]Department of Medicine, Division of Pulmonary, Allergy & Critical Care Medicine, University of Alabama at Birmingham, THT 422, 1720 2nd Avenue S., Birmingham, AL 35294-2182, USA

[4]These authors contributed equally

[5]Lead contact

SUMMARY

In injured airways of the adult lung, epithelial progenitors are called upon to repair by nearby mesenchymal cells via signals transmitted through the niche. Currently, it is unclear whether repair is coordinated by the mesenchymal cells that maintain the niche or by the airway epithelial cells that occupy it. Here, we show that the spatiotemporal expression of *Fgf10* by the niche is primarily orchestrated by the niche's epithelial occupants—both those that reside prior to, and following, injury. During homeostasis, differentiated airway epithelial cells secrete Sonic hedgehog (Shh) to inhibit *Fgf10* expression by $Gli1^{+}$ peribronchial mesenchymal cells in the niche. After injury, remaining epithelial cells produce Wnt7b to induce *Fgf10* expression in airway smooth muscle cells in the niche. We find that this reliance on a common activator of airway epithelial stem cells also allows for the recruitment of remote stem cell populations when local populations have been exhausted.

Graphical Abstract

*Correspondence: xiaokunli@wmu.edu.cn (X.L.), delanghe.stijn@mayo.edu (S.P.D.L.).

AUTHOR CONTRIBUTIONS

H.L. and R.W. designed and performed experiments, analyzed data, and wrote and edited the manuscript. S.G., T.Y., and K.K. performed experiments. J.-S.Z., D.B., and X.L edited the manuscript. S.P.D.L conceived and led the project, performed experiments, analyzed data, and wrote and edited the manuscript.

DECLARATION OF INTERESTS

The authors declare no competing interests.

SUPPLEMENTAL INFORMATION

Supplemental information can be found online at https://doi.org/10.1016/j.celrep.2022.111863.

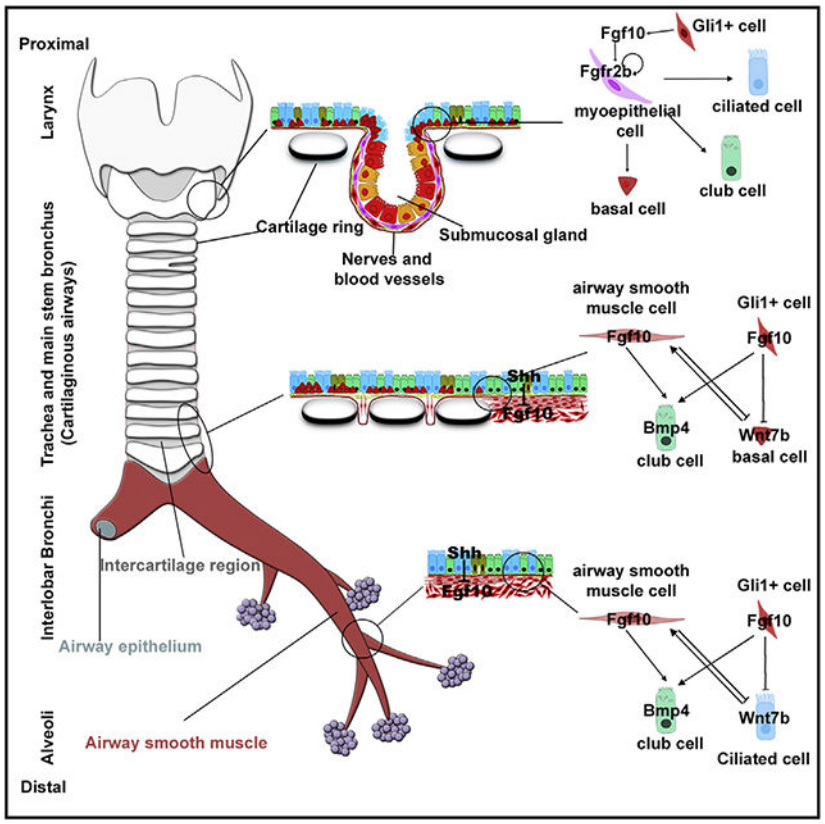

In brief

Lyu et al. show that complete activation of the peribronchial niche involves removal of an inhibitory Shh signal and initiation of an activating Wnt7b signal after airway injury. Communication between niches is required to synchronize airway epithelial regeneration and to restore quiescence in niche and progenitor cells during injury resolution.

INTRODUCTION

Epithelia provide a barrier to the outside world, and their disruption can result in various diseases. To function as an intact barrier, epithelia must maintain constant cell numbers despite sometimes high turnover rates. Stem/progenitor cells are required for tissue homeostasis and repair and reside in a highly specialized stromal microenvironment, called the stem cell niche,[1] where they are kept in a quiescent state during homeostasis or rapidly amplify upon tissue insults. Basal cells located in the protected environment of the cartilaginous airways of the trachea represent the main stem/progenitor cell population in the trachea. When activated, they self-renew or give rise to secretory club or ciliated cells.[2] Secretory club cells themselves can act as transit-amplifying cells but, in the conducting airway, also have the potential to self-renew or differentiate into post mitotic ciliated daughter cells or goblet cells.[3,4] Secretory cells drive almost the entire cell turnover in the distal conducting airways during homeostasis or repair of small injuries.[4]

Chronic diseases that lack the ability to restore injured organs to their normal structure and function, such as chronic obstructive pulmonary disease (COPD), asthma, and idiopathic pulmonary fibrosis (IPF), may have defects in stem/progenitor cell or niche function. For example, the first histological change to the airway epithelium associated with smoking is basal cell hyperplasia (squamous metaplasia), followed by loss of ciliated cells, shorter cilia, goblet cell hyperplasia, and loss of cell-cell junctions (with concomitant loss of barrier function).[5-12] An increase in basal cells has also been reported in individuals with asthma,[13,14] and there is overwhelming evidence for goblet cell metaplasia (GCM) in asthmatic conducting airways.[15-17]

In the lung, naphthalene (NPT) selectively destroys club cells along the entire conducting airway and ciliated cells in the proximal airways.[18-21] Traditionally, the NPT injury model has been used to study regeneration of the distal conducting airway epithelium, which is mostly mediated by surviving variant club cells, located at neuroepithelial bodies (NEBs) or bronchioalveolar duct junctions (BADJs),[22-25] but neuroendocrine cells[26,27] also play a role. Distal airway club cells are more multipotent than proximal club cells as demonstrated by their differential response to lung injury.[28-31] Yet, not much is known about the proximal-distal differences in airway epithelial regeneration or whether activation of different airway epithelial stem cells (AESCs) requires a different epithelial-mesenchymal crosstalk.

Previous studies have implicated epithelial-mesenchymal interactions in AESC activation after injury in the adult lung. Different models have been proposed; however, it is unclear how they affect proximal versus distal AESC populations and whether or how they integrate. The first model involves the release of a signal by surviving airway epithelial cells, sensing the loss of their neighbors, to activate the regenerative response. In this model, a decrease in cell density upon injury drives a Yap/Taz-mediated expression of *Wnt7b* in surviving airway ciliated epithelial cells, which then induces *Fgf10* expression in airway smooth muscle cells (ASMCs).[32-34] Fgf10 released by this ASMC niche then signals back to subsets of AESCs to drive airway epithelial regeneration. Interestingly, basal cells in the proximal airway also tonically produce Wnt7b to induce Fgf10 secretion by the niche, and Fgfr2b signaling is critical for their maintenance.[33-35] The second model of epithelial-mesenchymal crosstalk involves the removal of an inhibitory signal, previously secreted by the now-destroyed airway epithelial cells, to activate the regenerative response. In the second model, airway epithelial cells express *Sonic hedgehog (Shh)* during homeostasis to inhibit the expression of an unknown X-factor in the adjacent non-ASMC $Gli1^+$ peribronchial lung mesenchyme,[36] preventing this X-factor from activating the AESCs.

Interestingly, during lung development, Shh inhibits *Fgf10* expression in the lung mesenchyme,[37-41] suggesting that the X-factor inhibited by Shh in the Gli^+ mesenchyme might also be Fgf10. In the present study, we demonstrate that both ASMCs and $Gli1^+$ peribronchial mesenchymal cells maintain an Fgf10-producing niche. By inactivating *Fgf10* specifically in ASMCs or in $Gli1^+$ peribronchial mesenchyme, we demonstrate that Fgf10 coming from both niche-maintaining cell types is required for optimal airway epithelial regeneration after NPT injury. We further show that Fgf10 coming from this niche is required to promote basal to club cell differentiation, as inactivation of *Fgf10* in either niche-maintaining cell type impairs differentiation of basal cells into club cells. We further show

that both niche-maintaining cell types communicate with the niche occupants to synchronize airway epithelial regeneration by different AESCs, all requiring Fgf10, along the proximal-distal axis. Both niches are also necessary to return niche and AESC activation to baseline during injury resolution to restore quiescence. Lastly, we demonstrate an important role for Fgf10-Fgfr2b signaling in the recruitment of basal stem cells and submucosal myoepithelial stem cells to drive airway epithelial regeneration in the lung.

RESULTS

Two niche-maintaining cell types promote airway epithelial repair via Fgf10 expression

ASMCs and Gli1$^+$ peribronchial mesenchyme have both been described as mesenchymal AESC niche-maintaining cell types.[33-35,42,43] If the airway epithelium is the inner layer of a tube, the ASMCs would lay on top of this layer (i.e., middle layer) and the Gli1$^+$ peribronchial mesenchyme would be a third layer or outer layer. To investigate whether both niche-maintaining cell types produce Fgf10 to drive airway epithelial regeneration, we inactivated *Fgf10* prior to NPT injury in either the ASMCs (using *Acta2-CreERT2* or *Lgr6-CreERT*) or in the peribronchial mesenchymal cells (using *Gli1-CreERT2*) and monitored airway epithelial regeneration post injury. Interestingly, we found a need for Fgf10 coming from both mesenchymal niche-maintaining cell types to drive airway epithelial regeneration in the adult airway as regeneration was impaired upon inactivation of *Fgf10* in either niche-maintaining cell type (Figures 1A-1E, 1G, and 1H). To investigate the need for Fgf10 coming from both niche-maintaining cell types for airway epithelial regeneration, we also inactivated the receptor for Fgf10, *Fgfr2b*, in all airway epithelial cells using *Sox2-CreERT2*. As predicted, inactivation of *Fgfr2b* in all airway epithelial cells impaired airway epithelial regeneration more than inactivation of *Fgf10* in a single mesenchymal niche-maintaining cell type alone (Figures 1A-1E, 1G, and 1H), suggesting that in the latter case, Fgf10 coming from only one niche-maintaining cell type with or without the help of an alternate Fgfr2b ligand is still able to partially drive some airway epithelial regeneration, though at a slower rate.

Since our data indicate that Fgf10 coming from both niche-maintaining cell types is required for optimal airway epithelial regeneration, we wondered why such an apparently redundant system might have developed. We have previously shown that the ASMCs in the niche secrete Fgf10 after different types of injury such as NPT, ozone, and bleomycin.[34] As such, we hypothesized that different types of injury leave the AESC niche with different occupants along the proximal distal axis, which may activate the niche using different mechanisms. Interestingly, while NPT injury in the distal airway selectively ablates club cells, leaving surviving ciliated cells to secrete Wnt7b to induce *Fgf10* expression in the ASMCs of the niche, both club and ciliated cells are killed in the proximal airway (Figures 2A-2C). This lack of surviving club and ciliated cells in the proximal airway prevents the previously understood activation of the ASMC niche-maintaining cell type around the proximal conducting airways. We thus hypothesized that activation of the ASMC niche-maintaining cell type around the proximal airway and subsequent regeneration would require the expansion of rare basal cells in the proximal airways and/or the downward migration of basal cells, which also secrete Wnt7b.[33]

In order to identify which AESC populations are involved in proximal versus distal airway epithelial regeneration, we lineage traced club, basal, and neuroendocrine cells using *Scgb1a1-CreERT;mTmG, Krt5-CreERT2;mTmG*, and *Piezo2-Cre;mTmG* mice, respectively. We found that after NPT injury, ~80% of regenerated club cells in the distal airway are derived from previously existing club cells. However, to our surprise, we found that ~15% were derived from basal cells (Figures 2E and 2F). Interestingly, in the proximal airway, we found that ~75% of club cells were derived from basal cells, whereas only ~18% were derived from preexisting club cells (Figures 2E and 2F). Note that in the absence of injury, very few lineage-labeled basal cells are present in *Krt5-CreERT2;mTmG* lungs (Figures 2D and 2E), whereas in the trachea, we found that ~100% of club cells were derived from basal cells after injury, in line with previous reports[2] (Figure 2G). Finally, our data indicate that the participation of neuroendocrine cells in club cell regeneration is almost negligible (Figures 2E and 2F).

We have previously demonstrated that *Fgfr2b* signaling is essential for basal cell survival during homeostasis.[33,44] Since Fgf10 is known to function as a chemotactic factor,[45] our data therefore suggest that Fgf10 secreted by either niche-maintaining cell type may help recruit basal cells to the proximal airway to drive airway epithelial regeneration after NPT injury. Surprisingly, even though club cell regeneration was reduced in the proximal airways of all our different mutants, we only found fewer basal cells in the proximal airways of *Sox2-CreERT2;Fgfr2b*$^{f/f}$ mice (Figures 1F, 1I, and 1J) but not in the airways of mice in which we inactivated *Fgf10* in only one niche-maintaining cell type. Interestingly, we find that when *Fgf10* is inactivated in either niche-maintaining cell type, regenerated club cells feature higher Muc5b expression, indicative of proximal club cells (Figures 1K and 2H). In summary, we propose that both ASMCs and Gli1^{+} peribronchial mesenchymal niche-maintaining cell types secrete Fgf10 to drive proper airway epithelial regeneration. We further find that activation of both niche-maintaining cell types is required for optimal club cell regeneration but that basal stem cells can survive even when activation of one niche-maintaining cell type is impaired.

Club cells secrete Shh to suppress Fgf10 and epithelial regeneration

The Hedgehog (Hh) pathway coordinates tissue-tissue interactions through paracrine activation of smoothened (Smo)-mediated downstream signaling events.[46,47] In the adult lung epithelium, Shh is expressed predominantly in club cells in the proximal airway (Figure 1A), with scattered expression in ciliated and the alveolar type II cells.[36] The downstream transcriptional effector and target of Hh Gli1[48] is expressed predominantly in mesenchymal cells adjacent to the proximal airway and pulmonary artery,[36] with scattered expression in the alveolar interstitium. During lung development, Shh inhibits *Fgf10* expression in the lung mesenchyme,[37-41] suggesting that Shh might be inhibiting *Fgf10* expression in the Gli^{+} mesenchyme in the adult lung at homeostasis.

To investigate whether Fgf10 is the main signal inhibited by Shh in the Gli1^{+} peribronchial mesenchyme, we inactivated Smo using *Gli1-CreERT2* either alone or in combination with *Fgf10*. qPCR analysis indicates that *Fgf10* expression is upregulated in *Gli1-CreERT2;Smo*$^{f/f}$ lungs but downregulated in *Gli1-CreERT2;Smo*$^{f/f}$*;Fgf10*$^{f/f}$ lungs

(Figure 3A). As predicted, club cell regeneration after NPT injury was increased in *Gli1-CreERT2;Smo*$^{f/f}$ lungs, but this effect was negated in *Gli1-CreERT2;Smo*$^{f/f}$*;Fgf10*$^{f/f}$ lungs (Figures 3A, 3C-3E, and 3S). Interestingly, we found fewer basal cells, but more club cells, expressing less Muc5b, indicative of distal club cells, in the proximal airways of *Gli1-CreERT2;Smo*$^{f/f}$ lungs compared with control lungs at 1 and 3 week post NPT injury, and this effect was negated in *Gli1-CreERT2;Smo*$^{f/f}$*;Fgf10*$^{f/f}$ lungs (Figures 3A, 3F-3I, 3S, and 2M), suggesting that in the context of injury, Fgf10 promotes basal to club cell differentiation and inhibits Muc5b expression.

To further confirm the role of Shh in inhibiting *Fgf10* expression in the Gli1^{+} peribronchial mesenchyme, we also inactivated *Shh* in all airway epithelial cells or club cells using *Sox2-CreERT2, Scgb1a1-Cre*, and *Scgb1a1-CreERT*, respectively, alone or in combination with the receptor for Fgf10 *Fgfr2b* and found that *Fgf10* expression was upregulated in all mouse models, yet regeneration was only increased upon inactivation of *Shh* alone (Figures 3J-3N, 3S, and S1A-S1K). Interestingly, we found that airway epithelial regeneration in *Scgb1a1-Cre;Shh*$^{f/f}$*;Fgfr2b*$^{f/f}$ lungs in which *Fgfr2b* is inactivated only in club cells was less compromised than airway epithelial regeneration in *Sox2-CreERT2;Shh*$^{f/f}$*;Fgfr2b*$^{f/f}$ lungs (Figures 3J-3N, 3S, and S1A-S1K), indicating that the increased Fgf10 levels also promote club cell regeneration by basal cells. As a corollary, we also found fewer basal cells, but more club cells, expressing less Muc5b, indicative of distal club cells, in the airways of *Sox2-CreERT2;Shh*$^{f/f}$ mice in which *Fgf10* expression was induced in the peribronchial mesenchyme. However, since Fgfr2b signaling is critical for basal stem cell maintenance, basal cells were not present in *Sox2-CreERT2;Shh*$^{f/f}$*;Fgfr2b*$^{f/f}$ or *Sox2-CreERT2;Fgfr2b*$^{f/f}$ mice lungs after injury (Figures 3J, 3O-3Q, and 3S). Interestingly, inactivation of *Shh* or *Shh* and *Fgr2b* in club cells alone in *Scgb1a1-Cre;Shh*$^{f/f}$ or *Scgb1a1-Cre;Shh*$^{f/f}$*;Fgfr2b*$^{f/f}$ lungs, respectively, did not have a significant effect on basal cell abundance, but *Scgb1a1-Cre;Shh*$^{f/f}$ featured fewer club cells in the proximal airway after injury compared with control lungs (Figures S1A-S1K), suggesting that inactivation of Shh in all airway epithelial cells may be required to have complete activation of the niche. Together, these data suggest that club cells are not a major source of basal cells and that Shh secreted by niche occupants prior to injury primarily inhibits *Fgf10* expression in the peribronchial mesenchyme to maintain airway epithelial progenitor quiescence.

Feedback loops between Fgf10, Shh, and Wnt7b fine-tune airway epithelial regeneration

We have previously shown that surviving airway epithelial cells, sensing the loss of their neighbors upon NPT injury, release Wnt7b downstream of Yap/Taz to induce *Fgf10* expression in ASMCs.[32-34,42] Fgf10 released by this ASMC niche then signals back to subsets of AESCs to drive airway epithelial regeneration. When Shh-expressing club cells are destroyed due to NPT injury, *Fgf10* expression in the peribronchial mesenchyme becomes de-repressed. When club cells regenerate and cell density is restored, *Shh, Wnt7b*, and *Fgf10* expression should return to homeostatic levels.

Inherently, both niche-maintaining cell types communicate to fine-tune *Fgf10* expression levels by affecting *Shh* and *Wnt7b* expression. To investigate if both niche-maintaining cell types communicate with each other to fine-tune *Fgf10* expression levels, we determined

whether inactivation of *Shh* in all airway epithelial cells or club cells, or *Smo* inactivation in Gli1^{+} peribronchial mesenchyme, affected *Wnt7b* expression. We discovered that *Wnt7b* expression was downregulated in each mouse model compared with control lungs at 1 and 3 weeks post NPT injury (Figures 4A, 4D, and 4G), in line with an increase in cell density due to increased Fgf10-driven epithelial regeneration. As expected, we found that simultaneous inactivation of *Shh* and *Fgfr2b* in club cells or *Smo* and *Fgf10* in peribronchial mesenchyme negated these effects on *Wnt7b* expression. To further investigate whether Fgf10 inhibits *Wnt7b* expression, we checked *Wnt7b* expression levels in *Gli1-CreERT2;Fgf10$^{f/f}$*, *Acta2-CreERT2;Fgf10$^{f/f}$*, *Lgr6-CreERT2;Fgf10$^{f/f}$*, and *Lgr6-CreERT2;Ctnnb1$^{f/f}$* lungs and found *Wnt7b* to be upregulated post NPT injury in all these models that feature reduced *Fgf10* expression compared with control lungs (Figure 4A). Together, these findings indicate that Fgf10 coming from the Gli1^{+} peribronchial mesenchyme can inhibit *Wnt7b* expression by the epithelium to reduce *Fgf10* induction in ASMCs in order to fine-tune the combined Fgf10 output level by both niche-maintaining cell types. *Wnt7b* expression was similarly upregulated in lungs in which we inactivated *Fgfr2b* in all airway epithelial cells or club cells (Figures 4D and 4G). To verify that Fgf10 from both niches is indeed signaling to the airway epithelium, we performed qPCR, immunostaining, and/or signal amplification by exchange reaction-fluorescence *in situ* hybridization (SABER-FISH) for *Fgf10, Wnt7b*, and the Fgf10 epithelial target gene *Bmp4* on all our different mutant lungs and found that *Wnt7b* and *Bmp4* expression was diametrically regulated by Fgf10 (Figures 4A, 4B, 4D, 4E, 4G, 4H, and S2-S6).

We next wondered whether Fgf10 also regulates *Shh* expression. To investigate this, we monitored *Shh* expression levels in *Sox2-CreERT2;Wnt7b$^{f/f}$*, *Gli1-CreERT2;Fgf10$^{f/f}$*, *Acta2-CreERT2;Fgf10$^{f/f}$*, *Lgr6-CreERT2;Fgf10$^{f/f}$*, and *Lgr6-CreERT2;Ctnnb1$^{f/f}$* lungs and found *Shh* to be downregulated at 3, 7, and 21 days post NPT injury in all these models that feature reduced *Fgf10* expression, compared with control lungs, in line with a decrease lung regeneration and thus recovery of Shh-expressing club cells. We confirmed that *Sox2-CreERT2;Wnt7b$^{f/f}$* lungs and *Lgr6-CreERT2;Ctnnb1$^{f/f}$* lungs in which we knocked out *Wnt7b* in all airway epithelial cells or *β-catenin* in ASMCs, respectively, showed reduced *Fgf10* expression and club cell regeneration after NPT injury compared with control lungs (Figures 3A-3S). In addition, we found *Shh* to be upregulated in *Gli1-CreERT2;Smo$^{f/f}$* lungs, which feature increased *Fgf10* expression (Figures 4C, 4F, 4I, and S7-S8). Our data therefore suggest a dynamic and reciprocal crosstalk between the niche-maintaining cell types and its occupants to fine-tune *Fgf10* expression levels and AESC activation. Lastly, to rule out that Shh also signals directly to the epithelium, we inactivated or overexpressed *Smo* in the epithelium using *Scgb1a1-Cre;Smo$^{f/f}$* or *Sox2^{CreERT2};R26S-moM2* mice but found no difference between these mouse lines compared with controls in either club cell or basal cell abundance nor in *Fgf10* expression levels (Figures 4I and S9A-S9I).

Fgf10 activates different stem cell populations along the proximal distal axis

Recently, myoepithelial cells (MECs), a population of basal-like alpha-smooth muscle actin (α-SMA; Acta2^{+}), Krt5^{+}, and Krt14^{+} cells in submucosal glands (SMGs), have been revealed to serve as reserve stem cells for the tracheal surface airway epithelium (SAE), recruited from the protected SMG microenvironment whenever necessary to regenerate both

basal and luminal compartments in the tracheal SAE.[49,50] As such, tracheal SMGs are thought to serve as a protected stem cell niche, sequestering epithelial stem cells from the more exposed environment of the SAE. Given that SMGs can be found throughout the human airways, this stem cell niche may play a significant role in human lung regeneration and disease.

Interestingly, human SMGs stain strongly for Fgfr2 and Fgf10 (Figure 5A). suggesting that Fgf10-Fgfr2b signaling might drive MEC to SAE regeneration. To investigate this, we generated a mouse model in which we could specifically target lung epithelial cells that co-express the lung epithelial cell marker *Nkx2.1* and the mesenchymal *Acta2* (α-SMA) marker. To achieve this goal, we generated an *Acta2-Frt-STOP-Frt-Cre^{ERT2}* knockin mouse line. This line possesses a Cre^{ERT2} cassette inserted in the ATG start codon of the *Acta2* locus, which is preceded by a STOP codon, flanked by *Frt* sites. As such, when crossed with Flpo-expressing mice, *Acta2-Frt-STOP-Frt-Cre^{ERT2}* mice permanently express Cre^{ERT2} in the *Acta2* and *Flpo* co-expressing cells as well as their offspring due to the removal of the STOP codon. Thus, when an *Nkx2.1^{Flpo}* mouse[51] is crossed to an *Acta2-Frt-STOP-Frt-Cre^{ERT2}* mouse line, the progeny possesses the compound transgenes that allow for the removal of the STOP codon in lung epithelial cells. Our data indicate that we can specifically label MECs in the SMG using *Nkx2.1^{Flpo};Acta2-Frt-STOP-Frt-Cre^{ERT2};Rosa26^{mTmG}* mice (Figure 5B).

To investigate a role for Fgf10-Fgfr2b signaling in MEC to SAE differentiation, we inactivated *Fgfr2b* or *Fgf10* in MECs using *Nkx2.1^{Flpo};Acta2-Frt-STOP-Frt-Cre^{ERT2};Fgfr2b$^{f/f}$;Rosa26^{mTmG}* and *Nkx2.1^{Flpo};Acta2-Frt-STOP-Frt-Cre^{ERT2};Fgf10$^{f/f}$;Rosa26^{mTmG}* mice, respectively. We found that in control *Nkx2.1^{Flpo};Acta2-Frt-STOP-Frt-Cre^{ERT2};Rosa26^{mTmG}* mice, respectively. We found that in control *Nkx2.1^{Flpo};Acta2-Frt-STOP-Frt-Cre^{ERT2};Rosa26^{mTmG}* mice, MECs readily regenerate the SAE after NPT injury; however, upon inactivation of *Fgfr2b*, MECs failed to do so. To our surprise, however, we found that inactivation of Fgfr2b in MECs, unlike in basal cells, did not affect MEC maintenance. Inactivation of *Fgf10* in MECs, on the other hand, had no effect on SAE regeneration, suggesting that MECs do not produce Fgf10 themselves to signal in an autocrine fashion (Figures 5C-5E) despite their epithelial-mesenchymal-like nature. Instead, we find that Gli1^{+} peribronchial mesenchyme forms the *Fgf10*-expressing niche for MECs (Figure S10L).

Interestingly, we find that after NPT injury, even in the conducting airways of the lung, some basal cells in control and *Nkx2.1^{Flpo};Acta2-Frt-STOP-Frt-Cre^{ERT2};Fgf10$^{f/f}$;Rosa26^{mTmG}* lungs are derived from MECs, indicating migration of MEC daughter cells from the SMG into the lung; however, we could not find any labeled cells in the lungs of *Nkx2.1^{Flpo};Acta2-Frt-STOP-Frt-Cre^{ERT2};Fgfr2b$^{f/f}$;Rosa26^{mTmG}* mice (Figures 5C and 5F). Moreover, *Nkx2.1^{Flpo}Acta2-Frt-STOP-Frt-Cre^{ERT2};Fgfr2b$^{f/f}$;Rosa26^{mTmG}* mice featured fewer basal cells in general in the lung after NPT injury (Figures 5E and 5F), suggesting that when MECs cannot contribute to the repair of the SAE in the trachea, fewer basal cells are able to be recruited to regenerate the lung, likely due to these basal cells being retained or recruited to the trachea by a competing Fgf10 signal.

To investigate why MEC maintenance is not affected by the inactivation of *Fgfr2b*, we investigated the expression of Fgfr1 and Fgfr2b in MEC and basal cells (BCs) of the SMG and trachea using a mouse model featuring nuclear expression of cerulean under control of the Fgfr1 promoter and nuclear expression of mCherry under control the Fgfr2 promoter. Interestingly, we found that BCs, unlike previous reports,[35] only express *Fgfr2*, whereas MECs express both *Fgfr1* and *Fgfr2* (Figures S10A-S10K). In summary, we find that MECs are crucial stem cells for the repair of adult SMGs and also serve as reserve stem cells for the SAE of both trachea and lung. In response to injury, MECs are recruited from the SMG microenvironment whenever necessary to regenerate both basal and luminal compartments of the SAE of lung and trachea.

DISCUSSION

Here, we describe how ASMCs and Gli1$^+$ peribronchial mesenchymal cells form a compound niche, which is activated by diverse occupants of the niche along the proximal distal axis, to secrete Fgf10, which then functions as a common activator of different AESC populations along the proximal distal axis. We imagine that Fgf10 secreted by the niche also acts as a chemotactic factor to recruit remote AESCs to the site of injury[45] when local populations have been destroyed or exhausted.

Prior to injury, epithelial cells secrete Shh to inhibit Fgf10 secretion by the Gli1$^+$ peribronchial component of the niche. After injury, remaining surviving epithelial cells secrete Wnt7b to induce *Fgf10* expression in the ASMC component of the niche. Complete activation of the compound niche involves the removal of an inhibitory Shh signal previously secreted by the now-destroyed epithelial cells as well as the release of an activating signal, Wnt7b, by surviving epithelial cells sensing the loss of their neighbors. We further show that both components of the niche communicate with the niche occupants to synchronize airway epithelial regeneration by different airway epithelial progenitors requiring Fgf10 along the proximal-distal axis and to return niche and progenitor activation to baseline during injury resolution to restore quiescence (Figure 6).

Our finding of a profound presence of BCs in the mouse airway goes against dogma and would suggest that the absence of BCs in the mouse airway is likely due to lack of injury in laboratory mice housed in a protective environment. Interestingly, Fgf10 drives SMG and BC development and is important for their maintenance.[33,44,52] At the onset of lung and trachea initiation, Fgf10 is detected in the ventral mesenchyme of the trachea[53] and then becomes restricted to the intercartilage mesenchyme at later stages and into adulthood.[53] SMGs are severely reduced in number and size in Fgf10 heterozygotes.[52,54] Abnormal function of SMGs of the upper respiratory tract is associated with severe/fatal asthma and cystic fibrosis later in life.[55,56] However, despite the significance of SMGs for human respiratory diseases, little is known about the mechanisms that control their growth, differentiation, homeostasis, and regeneration during early postnatal and adult life.

Limitations of the study

Differences between human and mouse lungs may affect how regeneration happens in humans. For example, SMGs are found along the entire airway, and therefore MECs likely play an even more important role in lung regeneration in humans than in mouse.

STAR★METHODS

RESOURCE AVAILABILITY

Lead contact—Further information and requests for resources and reagents should be directed to and will be fulfilled by the lead contact, Stijn De Langhe: delanghe.stijn@mayo.edu.

Materials availability—Mouse lines generated in this study are available upon reasonable request.

Data and code availability—The data reported in this paper will be shared by the lead contact upon request.

This paper does not report original code.

Any additional information required to reanalyze the data reported in this paper is available from the lead contact upon request.

EXPERIMENTAL MODELS AND SUBJECT DETAILS

All mice were bred and maintained in a pathogen-free environment with free access to food and water. Both male and female mice were used for all experiments. *Fgfr2b*$^{f/f}$,[57] *Sox2*^{CreERT2} (JAX 017593), *Scgb1a1*^{CreER} (JAX 016225), *Scgb1a1*^{Cre},[58,59] *Rosa26-mTmG* (JAX 007676), *Rosa26-tdtomato* (JAX 007909), *Nkx2.1*^{Flpo} (JAX 028577), *Fgfr1*^{Cerulean} (JAX 030708), *Fgfr2*^{mCherry} (JAX 030710), *Krt5*^{CreERT2}[60], *Acta2*^{CreERT2},[61] *Fgf10*$^{f/f}$,[62] *Wnt7b*$^{f/f}$ (JAX 008467), *Lgr6*^{CreERT2} (JAX 016934), *Shh*$^{f/f}$ (JAX 004293), *Gli1*^{CreERT2} (JAX 007913), *Smo*$^{f/f}$ (JAX 004526), *R26SmoM2* (JAX 005130), and *Piezo2*^{Cre} (JAX 027719) mice were previously described. The *Acta2-Frt-STOP-Frt-Cre*^{ERT2} line possesses a Cre^{ERT2} cassette, inserted behind the ATG in the *Acta2* locus, and which is preceded by a STOP codon, flanked by *Frt* sites. All experiments were approved by the University of Alabama at Birmingham and Mayo Clinic Institutional animal care and use committees. Naphthalene (Sigma-Aldrich) was dissolved in corn oil at 30 mg/mL and administered intraperitoneally at 8 weeks of age, with doses adjusted to achieve a 95% decrease in the abundance of *Scgb1a1* mRNA in total lung RNA of WT mice at 3 days after injection. For tamoxifen induction, mice were placed on tamoxifen containing food (rodent diet with 400 mg/kg tamoxifen citrate; Harlan Teklad TD.130860) at 6–8 weeks of age for 2 to 3 weeks and received two additional intraperitoneal tamoxifen shots (0.20 mg/g body weight, Enzo Life Sciences) in the last week of tamoxifen citrate feed. Naphthalene was administered following a 3-week tamoxifen wash-out and lungs were harvested at 3, 7, and 21 days after naphthalene injury.

METHOD DETAILS

Immunohistochemistry and fluorescence—All staining was done on paraffin sections of formalin-fixed lungs or tracheas. Immunofluorescent staining was performed with the following primary antibodies: goat anti-Scgb1a1 (1:200; clone T-18; sc-9772; Santa Cruz Biotechnology Inc.), rabbit anti-Scgb1a1 (1:500; WRAB-CCSP; Seven Hills Bioreagents), mouse anti-α-Actin (1:500; clone 1A4; sc-32251; Santa Cruz Biotechnology Inc.), rabbit anti-FGF10 (1:1000; AP14882PU-N; Acris) (1:1000, ABN44, Millipore), chicken anti-GFP (1:250; GFP-1020; Aves Labs Inc.), rabbit anti-Keratin 5 (1:200; clone EP1601Y; MA5-14473; Thermo Fisher Scientific), chicken anti-Keratin 5 (1:500; clone Poly9059; 905904; BioLegend), rabbit anti-Muc5b (1:500; B1914;Santa Cruz Biotechnology Inc.), rabbit anti-BMP4 (1:500, BS-1374R, Bioss Inc), mouse anti-SHH (1:50, sc-36512, Santa Cruz Biotechnology Inc.). After deparaffinization, slides were rehydrated through a series of decreasing ethanol concentrations, antigen unmasking by either microwaving in citrate-based antigen unmasking solution (Vector Labs, H-3000) or by incubating sections with proteinase K (7.5μg/mL) (Invitrogen, 25530–049) for 7 min at 37°C. Tissue sections were then washed in TBS with 0.1% Tween-20 and blocked with 3% Bovine Serum Albumin (BSA), 0.4% Triton in TBS for 30 min at room temperature followed by overnight incubation of primary antibodies diluted in 3% BSA, 0.1% Triton in TBS. The next day, slides were washed in TBS with 0.1% Tween-20 and incubated with secondary antibodies diluted in 3% BSA, 0.1% Triton in TBS for 3h at room temperature. All fluorescent staining was performed with appropriate secondary antibodies from Jackson Immunoresearch. Slides were mounted using Vectashield with (Vector Labs, H-1200) or without DAPI (Vector Labs, H-1000) depending on immunostaining.

Microscopy and imaging—Tissue was imaged using a micrometer slide calibrated Zeiss LSM800 Laser scanning confocal microscope using ZEN imaging software. In the lung, cells were counted using tiled stitched 20x images covering the entire cross-section of the lower right lung lobe or trachea from ≥6 different lungs/tracheas. Images were processed and analyzed using Zen blue (Zeiss) and Adobe Photoshop Creative Suite 3 (Adobe) software. Differentiation of GFP positive cells was determined by quantifying the total number of GFP+ cells that also showed a DAPI stained nucleus, and how many of those were Scgb1a1 and/or Krt5 positive. Image quantification and analysis was performed in a double blinded fashion. To calculate percent airway coverage, we measured the length of the airway and the length of the regenerated areas vs non regenerated areas based on Scgb1a1 or Krt5 immunostaining.

Quantitative real-time PCR—Total mRNA was extracted from lung accessory lobes stored in RNAlater (Invitrogen, AM7021) and using Total RNA Kit I (Omega Biotek, R6834-02) according to the manufacturer's instructions. RNA concentration was determined by spectrophotometry. cDNA was generated using Maxima™ First Strand cDNA Synthesis (Fisher Scientific, FERK1642) according to the manufacturer's instructions. Gene expression was analyzed by quantitative RT-PCR using Taqman Gene Expression Assays (Applied Biosystems, 4369016) directed against the mouse targets *β-glucuronidase* (Mm00446953_m1), *Keratin 5* (K5) (Mm01305291_g1), *p63 (Trp63)* (Mm00495788_m1), *Scgb1a1* (Mm00442046_m1), *Muc5b* (Mm00466391_m1), *Fgf10* (Mm00433275_m1),

Wnt7b (Mm00437358_m1), *Bmp4* (Mm00432087_m1), and *Shh* (Mm00436528_m1). Quantitative real-time PCR was performed using a StepOne Plus system (Applied Biosystems). Data were presented as expression relative to the housekeeping gene β-glucuronidase ± standard error of mean (SEM). Each experiment was repeated with samples obtained from at least 3 different lung preparations.

SABER-FISH—Signal Amplification By Exchange Reaction (SABER)[63] *in situ* fluorescence staining for *Wnt7b, Shh, Fgf10* and *Bmp4* was performed on formalin fixed paraffin embedded lung sections. Probes were designed using the OligoMiner pipeline using the mm10 whole-genome probe set from https://yin.hms.harvard.edu/oligoMiner/list.html. Probes targeting exons of desired genes were chosen based on the UCSC Genome Brower. Reverse complement sequences were combined with a "ttt" linker followed by a 9-mer primer sequence at the 3' end (Table S1). Each 9-mer primer sequence is unique for each gene, lacks sequence similarity to mm10, and do not contain G bases to minimize secondary structure and permit GC pairs to be used as a polymerase terminator sequence within the hairpin in the absence of dGTP in the reaction. Individual probe sets were pooled in equal amounts. The 9-mer primer sequence was extended using primer-exchange reaction (PER) using a hairpin containing the reverse complement of the 9-mer sequence, a "GGGCCTTTGGCCC" hairpin sequence, 2 repeats of the 9-mer sequence, followed by 3' InvdT. Branches were designed to bind the to extended 9-mer sequence of the primary probes with 3 repeating 9-mer reverse complement sequences followed by a "ttt" and a unique 9-mer sequence. Branches were also extended using PER. Primary probes were ordered from IDT in a 96-well plate format and branches and hairpins in individual tubes.

Prior to PER, the hairpins and branches were incubated with a "Clean G" sequence to remove all possible contaminating dGTP in the reaction. The PER was optimized for each probe and branch with varying concentrations of probe pool/branch, $MgSO_4$, hairpin, and extension time. To detect extension, the PER was run on a 1.25% agarose gel. When probe lengths reached 500–650nt and branches 250–450nt, the reactions were purified using MinElute PCR purification column (Qiagen). Probe/branch concentrations were determined by spectrophotometry.

Formalin-fixed paraffin embedded tissues were sectioned, deparaffinized, and rehydrated. Target retrieval was performed by incubating sections with proteinase K (7.5μg/mL) (Invitrogen, 25530–049) for 7 min at 37°C. Sections were then washed quickly with 2x SSC, 1% Tween-20, 40% formamide and then incubated with 2x SSC, 1% Tween-20, 40% formamide, 10% dextran sulfate, and primary probe (1ug/sample) for 16 h at 43°C. Sections were then washed quickly with 2x SSC, 1% Tween-20, 40% formamide, twice for 30 min with 2x SSC, 1% Tween-20, 40% formamide, and twice for 5 min with 2x SSC. In a similar manner, branching was performed for a total of 2 branchings per probe.

After branching, fluorescent detection and imaging were performed. Fluorescent imagers were designed to contain a 5' dye and 2 repeats of the reverse complement to the 9-mer extended sequence of the last branch added to the probe. The imagers were ordered from IDT with HPLC purification. Fluorescent detection was performed by incubating the section with 1x PBS, 0.2% Tween-20, 10% dextran sulfate, and 1μM fluorescent imager for 2 h at

37°C. Slides were then washed twice with 1x PBS, 0.1% Tween-20 and imaged as noted above.

QUANTIFICATION AND STATISTICAL ANALYSIS

All results are expressed as mean values ± SEM. The ‘n’ represents biological replicates and can be found in the figure legends. The significance of differences between 2 sample means was determined by unpaired student’s t-test (assuming unequal or equal variances as determined by the F-test of equality of variances) or ANNOVA with (Benjamini, Krieger and Yekutieli posthoc). The precise test used can be found in the figure legends. All datasets followed a normal distribution and p values less than 0.05 were considered statistically significant. The number of samples to be used was based on the number of experimental paradigms multiplied by the number in each group that is necessary to yield statistically significant results (based on power analysis, to reject the null hypothesis with 80% power (type I error = 0.05).

Supplementary Material

Refer to Web version on PubMed Central for supplementary material.

ACKNOWLEDGMENTS

This study was supported by NIH R01 HL126732, HL146461, HL132156 and R35 HL161169 to S.P.D.L. R.W. was supported by NIH T32 HL105346.

REFERENCES

1. Scadden DT (2006). The stem-cell niche as an entity of action. Nature 441, 1075–1079. [PubMed: 16810242]
2. Rock JR, Onaitis MW, Rawlins EL, Lu Y, Clark CP, Xue Y, Randell SH, and Hogan BLM (2009). Basal cells as stem cells of the mouse trachea and human airway epithelium. Proc. Natl. Acad. Sci. USA 106, 12771–12775. [PubMed: 19625615]
3. Pardo-Saganta A, Tata PR, Law BM, Saez B, Chow RDW, Prabhu M, Gridley T, and Rajagopal J (2015). Parent stem cells can serve as niches for their daughter cells. Nature 523, 597–601. [PubMed: 26147083]
4. Rawlins EL, Okubo T, Xue Y, Brass DM, Auten RL, Hasegawa H, Wang F, and Hogan BLM (2009). The role of Scgb1a1+ Clara cells in the long-term maintenance and repair of lung airway, but not alveolar, epithelium. Cell Stem Cell 4, 525–534. [PubMed: 19497281]
5. Auerbach O, Stout AP, Hammond EC, and Garfinkel L (1961). Changes in bronchial epithelium in relation to cigarette smoking and in relation to lung cancer. N. Engl. J. Med 265, 253–267. [PubMed: 13685078]
6. Lumsden AB, McLean A, and Lamb D (1984). Goblet and Clara cells of human distal airways: evidence for smoking induced changes in their numbers. Thorax 39, 844–849. [PubMed: 6505991]
7. Leopold PL, O’Mahony MJ, Lian XJ, Tilley AE, Harvey BG, and Crystal RG (2009). Smoking is associated with shortened airway cilia. PLoS One 4, e8157. [PubMed: 20016779]
8. Kennedy SM, Elwood RK, Wiggs BJ, Paré PD, and Hogg JC (1984). Increased airway mucosal permeability of smokers. Relationship to airway reactivity. Am. Rev. Respir. Dis 129, 143–148. [PubMed: 6142669]
9. Dye JA, and Adler KB (1994). Effects of cigarette smoke on epithelial cells of the respiratory tract. Thorax 49, 825–834. [PubMed: 8091331]

10. Peters EJ, Morice R, Benner SE, Lippman S, Lukeman J, Lee JS, Ro JY, and Hong WK (1993). Squamous metaplasia of the bronchial mucosa and its relationship to smoking. Chest 103, 1429–1432. [PubMed: 8486022]

11. Shaykhiev R, Otaki F, Bonsu P, Dang DT, Teater M, Strulovici-Barel Y, Salit J, Harvey BG, and Crystal RG (2011). Cigarette smoking reprograms apical junctional complex molecular architecture in the human airway epithelium in vivo. Cell. Mol. Life Sci 68, 877–892. [PubMed: 20820852]

12. Shaykhiev R, and Crystal RG (2014). Basal cell origins of smoking-induced airway epithelial disorders. Cell Cycle 13, 341–342. [PubMed: 24335435]

13. Hackett TL, Warner SM, Stefanowicz D, Shaheen F, Pechkovsky DV, Murray LA, Argentieri R, Kicic A, Stick SM, Bai TR, and Knight DA (2009). Induction of epithelial-mesenchymal transition in primary airway epithelial cells from patients with asthma by transforming growth factor-beta1. Am. J. Respir. Crit. Care Med 180, 122–133. [PubMed: 19406982]

14. Hackett TL, Shaheen F, Johnson A, Wadsworth S, Pechkovsky DV, Jacoby DB, Kicic A, Stick SM, and Knight DA (2008). Characterization of side population cells from human airway epithelium. Stem Cell. 26, 2576–2585.

15. Shimura S, Andoh Y, Haraguchi M, and Shirato K (1996). Continuity of airway goblet cells and intraluminal mucus in the airways of patients with bronchial asthma. Eur. Respir. J 9, 1395–1401. [PubMed: 8836649]

16. Jeffery P, and Zhu J (2002). Mucin-producing elements and inflammatory cells. Novartis Found. Symp 248, 51–68. discussion 68-75, 277-282. [PubMed: 12568488]

17. Ordoñez CL, Khashayar R, Wong HH, Ferrando R, Wu R, Hyde DM, Hotchkiss JA, Zhang Y, Novikov A, Dolganov G, and Fahy JV (2001). Mild and moderate asthma is associated with airway goblet cell hyperplasia and abnormalities in mucin gene expression. Am. J. Respir. Crit. Care Med 163, 517–523. [PubMed: 11179133]

18. Cole BB, Smith RW, Jenkins KM, Graham BB, Reynolds PR, and Reynolds SD (2010). Tracheal Basal cells: a facultative progenitor cell pool. Am. J. Pathol 177, 362–376. [PubMed: 20522644]

19. Mahvi D, Bank H, and Harley R (1977). Morphology of a naphthalene-induced bronchiolar lesion. Am. J. Pathol 86, 558–572. [PubMed: 842612]

20. Fanucchi M, Glaspy J, Crawford J, Garst J, Figlin R, Sheridan W, Menchaca D, Tomita D, Ozer H, and Harker L (1997). Effects of polyethylene glycol-conjugated recombinant human megakaryocyte growth and development factor on platelet counts after chemotherapy for lung cancer. N. Engl. J. Med 336, 404–409. [PubMed: 9010146]

21. Boyd MR (1977). Evidence for the Clara cell as a site of cytochrome P450-dependent mixed-function oxidase activity in lung. Nature 269, 713–715. [PubMed: 593334]

22. Giangreco A, Reynolds SD, and Stripp BR (2002). Terminal bronchioles harbor a unique airway stem cell population that localizes to the bronchoalveolar duct junction. Am. J. Pathol 161, 173–182. [PubMed: 12107102]

23. Hong KU, Reynolds SD, Giangreco A, Hurley CM, and Stripp BR (2001). Clara cell secretory protein-expressing cells of the airway neuroepithelial body microenvironment include a label-retaining subset and are critical for epithelial renewal after progenitor cell depletion. Am. J. Respir. Cell Mol. Biol 24, 671–681. [PubMed: 11415931]

24. Reynolds SD, Hong KU, Giangreco A, Mango GW, Guron C, Morimoto Y, and Stripp BR (2000). Conditional clara cell ablation reveals a self-renewing progenitor function of pulmonary neuroendocrine cells. Am. J. Physiol. Lung Cell Mol. Physiol 278, L1256–L1263. [PubMed: 10835332]

25. Reynolds SD, Giangreco A, Power JH, and Stripp BR (2000). Neuroepithelial bodies of pulmonary airways serve as a reservoir of progenitor cells capable of epithelial regeneration. Am. J. Pathol 156, 269–278. [PubMed: 10623675]

26. Song H, Yao E, Lin C, Gacayan R, Chen MH, and Chuang PT (2012). Functional characterization of pulmonary neuroendocrine cells in lung development, injury, and tumorigenesis. Proc. Natl. Acad. Sci. USA 109, 17531–17536. [PubMed: 23047698]

27. Ouadah Y, Rojas ER, Riordan DP, Capostagno S, Kuo CS, and Krasnow MA (2019). Rare pulmonary neuroendocrine cells are stem cells regulated by Rb, p53, and notch. Cell 179, 403–416.e23. [PubMed: 31585080]
28. Kim CFB, Jackson EL, Woolfenden AE, Lawrence S, Babar I, Vogel S, Crowley D, Bronson RT, and Jacks T (2005). Identification of bronchioalveolar stem cells in normal lung and lung cancer. Cell 121, 823–835. [PubMed: 15960971]
29. Lee JH, Bhang DH, Beede A, Huang TL, Stripp BR, Bloch KD, Wagers AJ, Tseng YH, Ryeom S, and Kim CF (2014). Lung stem cell differentiation in mice directed by endothelial cells via a BMP4-NFATc1-thrombospondin-1 Axis. Cell 156, 440–455. [PubMed: 24485453]
30. Salwig I, Spitznagel B, Vazquez-Armendariz AI, Khalooghi K, Guenther S, Herold S, Szibor M, and Braun T (2019). Bronchioalveolar stem cells are a main source for regeneration of distal lung epithelia in vivo. EMBO J. 38, e102099. [PubMed: 31028085]
31. Liu Q, Liu K, Cui G, Huang X, Yao S, Guo W, Qin Z, Li Y, Yang R, Pu W, et al. (2019). Lung regeneration by multipotent stem cells residing at the bronchioalveolar-duct junction. Nat. Genet 51, 728–738. [PubMed: 30778223]
32. Rock JR, Gao X, Xue Y, Randell SH, Kong YY, and Hogan BLM (2011). Notch-dependent differentiation of adult airway basal stem cells. Cell Stem Cell 8, 639–648. [PubMed: 21624809]
33. Volckaert T, Yuan T, Chao CM, Bell H, Sitaula A, Szimmtenings L, El Agha E, Chanda D, Majka S, Bellusci S, et al. (2017). Fgf10-Hippo epithelial-mesenchymal crosstalk maintains and recruits lung basal stem cells. Dev. Cell 43, 48–59.e5. [PubMed: 29017029]
34. Volckaert T, Dill E, Campbell A, Tiozzo C, Majka S, Bellusci S, and De Langhe SP (2011). Parabronchial smooth muscle constitutes an airway epithelial stem cell niche in the mouse lung after injury. J. Clin. Invest 121, 4409–4419. [PubMed: 21985786]
35. Balasooriya GI, Goschorska M, Piddini E, and Rawlins EL (2017). FGFR2 is required for airway basal cell self-renewal and terminal differentiation. Development 144, 1600–1606. [PubMed: 28348168]
36. Peng T, Frank DB, Kadzik RS, Morley MP, Rathi KS, Wang T, Zhou S, Cheng L, Lu MM, and Morrisey EE (2015). Hedgehog actively maintains adult lung quiescence and regulates repair and regeneration. Nature 526, 578–582. [PubMed: 26436454]
37. Bellusci S, Furuta Y, Rush MG, Henderson R, Winnier G, and Hogan BL (1997). Involvement of Sonic hedgehog (Shh) in mouse embryonic lung growth and morphogenesis. Development 124, 53–63. [PubMed: 9006067]
38. White AC, Xu J, Yin Y, Smith C, Schmid G, and Ornitz DM (2006). FGF9 and SHH signaling coordinate lung growth and development through regulation of distinct mesenchymal domains. Development 133, 1507–1517. [PubMed: 16540513]
39. Pepicelli CV, Lewis PM, and McMahon AP (1998). Sonic hedgehog regulates branching morphogenesis in the mammalian lung. Curr. Biol 8, 1083–1086. [PubMed: 9768363]
40. Hines EA, and Sun X (2014). Tissue crosstalk in lung development. J. Cell. Biochem 115, 1469–1477. [PubMed: 24644090]
41. Volckaert T, and De Langhe SP (2015). Wnt and FGF mediated epithelial-mesenchymal crosstalk during lung development. Dev. Dynam 244, 342–366.
42. Volckaert T, Campbell A, and De Langhe S (2013). c-Myc regulates proliferation and Fgf10 expression in airway smooth muscle after airway epithelial injury in mouse. PLoS One 8, e71426. [PubMed: 23967208]
43. Lee JH, Tammela T, Hofree M, Choi J, Marjanovic ND, Han S, Canner D, Wu K, Paschini M, Bhang DH, et al. (2017). Anatomically and functionally distinct lung mesenchymal populations marked by Lgr5 and Lgr6. Cell 170, 1149–1163.e12. [PubMed: 28886383]
44. Volckaert T, Campbell A, Dill E, Li C, Minoo P, and De Langhe S (2013). Localized Fgf10 expression is not required for lung branching morphogenesis but prevents differentiation of epithelial progenitors. Development 140, 3731–3742. [PubMed: 23924632]
45. Park WY, Miranda B, Lebeche D, Hashimoto G, and Cardoso WV (1998). FGF-10 is a chemotactic factor for distal epithelial buds during lung development. Dev. Biol 201, 125–134. [PubMed: 9740653]

46. McMahon AP, Ingham PW, and Tabin CJ (2003). Developmental roles and clinical significance of hedgehog signaling. Curr. Top. Dev. Biol 53, 1–114. [PubMed: 12509125]
47. Lum L, and Beachy PA (2004). The Hedgehog response network: sensors, switches, and routers. Science 304, 1755–1759. [PubMed: 15205520]
48. Bai CB, Auerbach W, Lee JS, Stephen D, and Joyner AL (2002). Gli2, but not Gli1, is required for initial Shh signaling and ectopic activation of the Shh pathway. Development 129, 4753–4761. [PubMed: 12361967]
49. Tata A, Kobayashi Y, Chow RD, Tran J, Desai A, Massri AJ, McCord TJ, Gunn MD, and Tata PR (2018). Myoepithelial cells of submucosal glands can function as reserve stem cells to regenerate airways after injury. Cell Stem Cell 22, 668–683.e6. [PubMed: 29656943]
50. Lynch TJ, Anderson PJ, Rotti PG, Tyler SR, Crooke AK, Choi SH, Montoro DT, Silverman CL, Shahin W, Zhao R, et al. (2018). Submucosal gland myoepithelial cells are reserve stem cells that can regenerate mouse tracheal epithelium. Cell Stem Cell 22. 779–667.
51. He M, Tucciarone J, Lee S, Nigro MJ, Kim Y, Levine JM, Kelly SM, Krugikov I, Wu P, Chen Y, et al. (2016). Strategies and tools for combinatorial targeting of GABAergic neurons in mouse cerebral cortex. Neuron 92, 555–1243.
52. Rawlins EL, and Hogan BLM (2005). Intercellular growth factor signaling and the development of mouse tracheal submucosal glands. Dev. Dynam 233, 1378–1385.
53. Sala FG, Del Moral PM, Tiozzo C, Alam DA, Warburton D, Grikscheit T, Veltmaat JM, and Bellusci S (2011). FGF10 controls the patterning of the tracheal cartilage rings via Shh. Development 138, 273–282. [PubMed: 21148187]
54. Jaskoll T, Abichaker G, Witcher D, Sala FG, Bellusci S, Hajihosseini MK, and Melnick M (2005). FGF10/FGFR2b signaling plays essential roles during in vivo embryonic submandibular salivary gland morphogenesis. BMC Dev. Biol 5, 11. [PubMed: 15972105]
55. Benayoun L, Druilhe A, Dombret MC, Aubier M, and Pretolani M (2003). Airway structural alterations selectively associated with severe asthma. Am. J. Respir. Crit. Care Med 167, 1360–1368. [PubMed: 12531777]
56. Salinas D, Haggie PM, Thiagarajah JR, Song Y, Rosbe K, Finkbeiner WE, Nielson DW, and Verkman AS (2005). Submucosal gland dysfunction as a primary defect in cystic fibrosis. Faseb. J 19, 431–433. [PubMed: 15596485]
57. De Moerlooze L, Spencer-Dene B, Revest JM, Hajihosseini M, Rosewell I, and Dickson C (2000). An important role for the IIIb isoform of fibroblast growth factor receptor 2 (FGFR2) in mesenchymal-epithelial signalling during mouse organogenesis. Development 127, 483–492. [PubMed: 10631169]
58. Ji H, Houghton AM, Mariani TJ, Perera S, Kim CB, Padera R, Tonon G, McNamara K, Marconcini LA, Hezel A, et al. (2006). K-ras activation generates an inflammatory response in lung tumors. Oncogene 25, 2105–2112. [PubMed: 16288213]
59. Simon DM, and Mariani TJ (2007). Role of PPARs and retinoid X receptors in the regulation of lung maturation and development. PPAR Res. 2007, 91240. [PubMed: 17710236]
60. Van Keymeulen A, Rocha AS, Ousset M, Beck B, Bouvencourt G, Rock J, Sharma N, Dekoninck S, and Blanpain C (2011). Distinct stem cells contribute to mammary gland development and maintenance. Nature 479, 189–193. [PubMed: 21983963]
61. Wendling O, Bornert JM, Chambon P, and Metzger D (2009). Efficient temporally-controlled targeted mutagenesis in smooth muscle cells of the adult mouse. Genesis 47, 14–18. [PubMed: 18942088]
62. Urness LD, Paxton CN, Wang X, Schoenwolf GC, and Mansour SL (2010). FGF signaling regulates otic placode induction and refinement by controlling both ectodermal target genes and hindbrain Wnt8a. Dev. Biol 340, 595–604. [PubMed: 20171206]
63. Kishi JY, Lapan SW, Beliveau BJ, West ER, Zhu A, Sasaki HM, Saka SK, Wang Y, Cepko CL, and Yin P (2019). SABER amplifies FISH: enchanced multiplexed imaging of RNA and DNA in cells and tissues. Nat. Methods 16, 533–544. [PubMed: 31110282]

Highlights

- ASMCs and Gli1^{+} peribronchial mesenchyme form the Fgf10 niche
- Shh from airway epithelial cells maintain niche Fgf10 levels, and vice versa
- Fgf10 from both ASMCs and Gli1^{+} cells is required for airway regeneration after NPT
- Fgfr2b is necessary in myoepithelial cells for their recruitment after injury

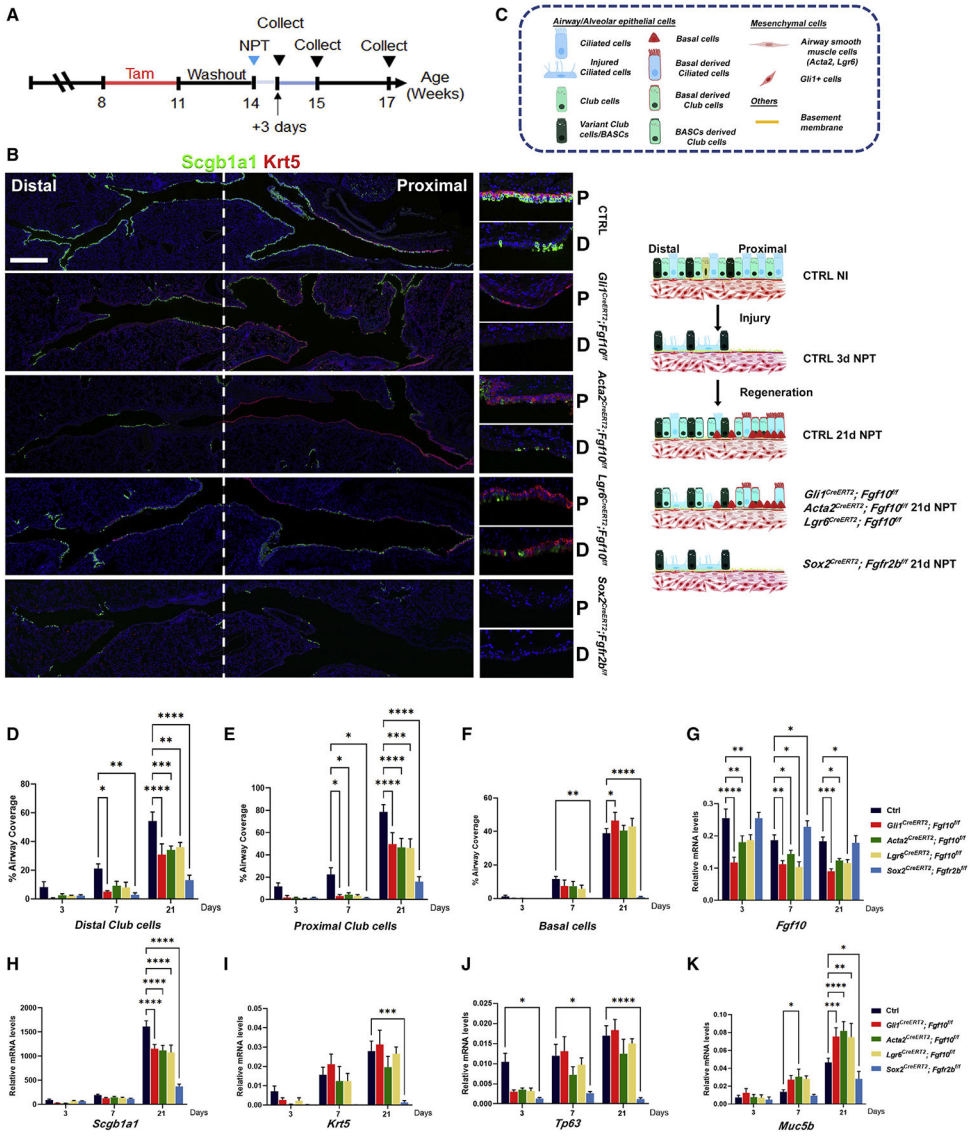

Figure 1. Two niche-maintaining cell types promote airway epithelial repair via *Fgf10* expression

(A) Schematic representation of experimental design: mice were placed on tamoxifen chow for 3 weeks starting at 8 weeks of age. After a 3 week washout period, mice were intraperitoneally (i.p.) injected with NPT at 20 weeks of age, and lungs were isolated at 3, 7, or 21 days after injury.

(B) Immunostaining for club and basal cell markers Scgb1a1 and Krt5, respectively, on control, *Gli1*^{CreERT2};*Fgf10*$^{f/f}$, *Acta2*^{CreERT2};*Fgf10*$^{f/f}$, *Lgr6*^{CreERT2};*Fgf10*$^{f/f}$, and *Sox2*^{CreERT2};*Fgfr2b*$^{f/f}$ mice 21 days after naphthalene injury. Higher-magnification panels on the right of proximal (P) versus distal (D) parts of the airway.

(C) Schematic representation of data presented in (B).

(D–F) Quantification of the percentage of the airway epithelium covered by club or basal cells in control, *Gli1*^{CreERT2};*Fgf10*$^{f/f}$, *Acta2*^{CreERT2};*Fgf10*$^{f/f}$, *Lgr6*^{CreERT2};*Fgf10*$^{f/f}$, and *Sox2*^{CreERT2};*Fgfr2b*$^{f/f}$ mice 3, 7, and 21 days after naphthalene injury.

(G–K) Relative mRNA expression of *Fgf10*, *Scgb1a1*, *Krt5*, *Tp63*, and *Muc5b* in control, *Gli1*^{CreERT2};*Fgf10*$^{f/f}$, *Acta2*^{CreERT2};*Fgf10*$^{f/f}$, *Lgr6*^{CreERT2};*Fgf10*$^{f/f}$, and *Sox2*^{CreERT2};*Fgfr2b*$^{f/f}$ mice 3, 7, and 21 days after naphthalene injury.
**p < 0.01; *p < 0.05. n ≥ 6.; error bars mean ± SEM. Scale bars, 500 μm. Two-sided t test and ANOVA used to determine statistical significance.

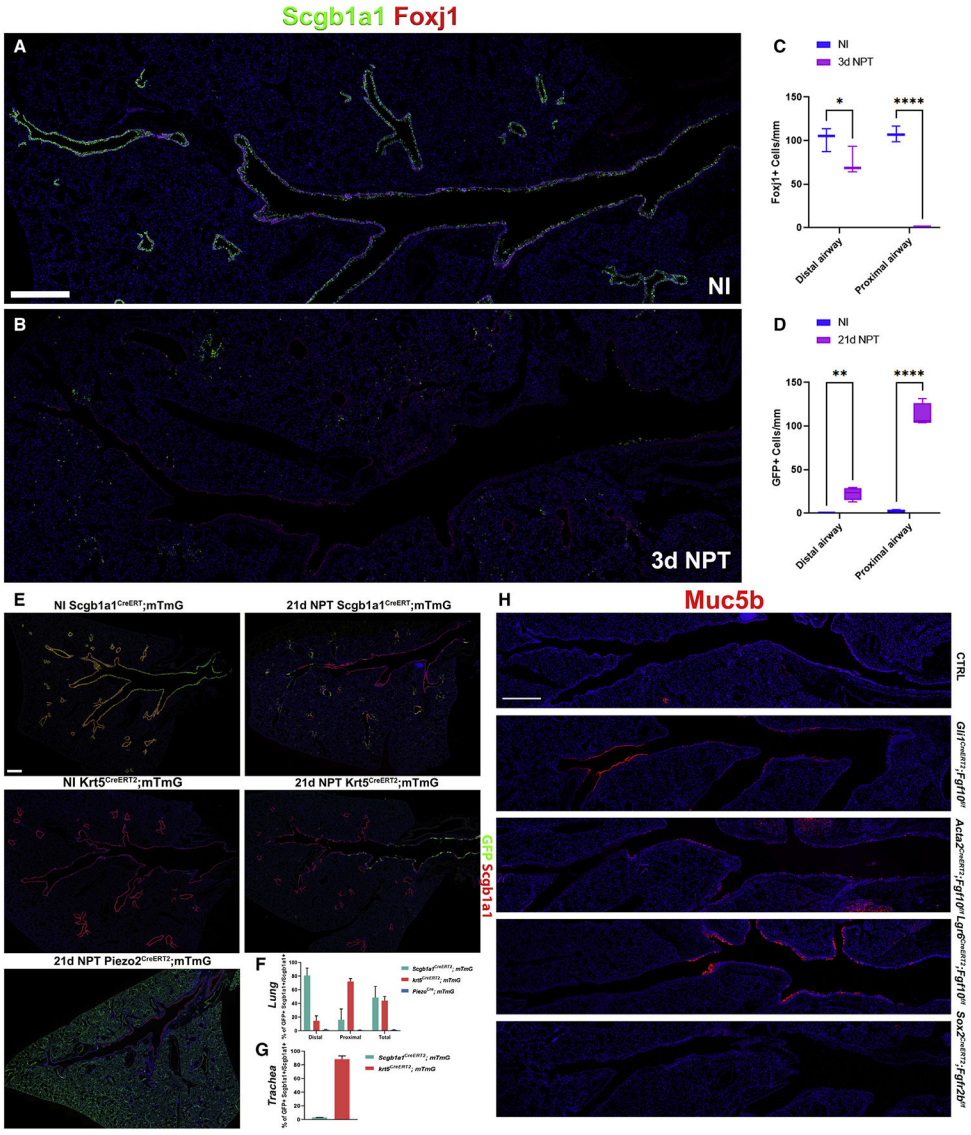

Figure 2. Distinct occupants along the proximal distal axis activate the airway stem cell niche to secrete Fgf10

(A and B) Immunostaining for club and ciliated cell markers Scgb1a1 and Foxj1, respectively, on control lungs without injury or at 3 days post naphthalene injury.

(C) Quantification of the number of ciliated cells per 1 mm of proximal or distal airway in non-injured lungs versus lungs 3 days after naphthalene injury.

(E) Immunostaining for GFP and club cell marker Scgb1a1 on *Scgb1a1*^{CreERT};*mTmG*, *Piezo2*^{Cre};*mTmG* and *Krt5*^{CreERT2};*mTmG* mice in which we lineage traced club cells, neuroendocrine cells, and basal cells, respectively, without injury or up to 21 days after naphthalene injury.

(F and G) Quantification of the percentage of club cells that are GFP labeled in each of the lineage-tracing models represented in (C) in lung and trachea.

(H) Immunostaining for Muc5b on control *Gli1*^{CreERT2};*Fgf10*$^{f/f}$, *Acta2*^{CreERT2};*Fgf10*$^{f/f}$, *Lgr6*^{CreERT2};*Fgf10*$^{f/f}$, and **Sox2**$^{\mathbf{CreERT2}}$;*Fgfr2b*$^{f/f}$ mice.

**p < 0.01; *p < 0.05. n ≥ 6.; error bars mean ± SEM. Scale bars, 500 μm. Two-sided t test and ANOVA used to determine statistical significance.

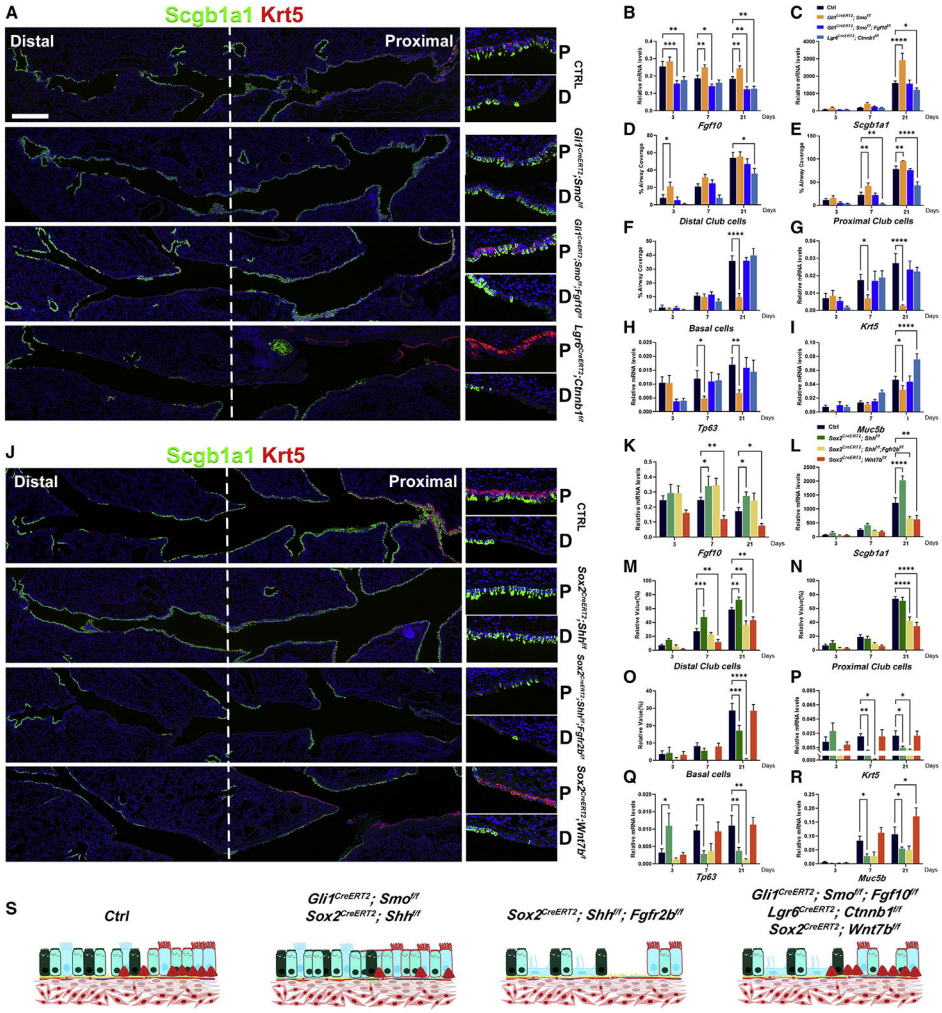

Figure 3. Club cells secrete Shh to suppress *Fgf10* and epithelial regeneration

(A and J) Immunostaining for club and basal cell markers Scgb1a1 and Krt5, respectively, on control, *Gli1*^{CreERT2};*Smo*$^{f/f}$, *Gli1*^{CreERT2};*Smo*$^{f/f}$,*Fgf10*$^{f/f}$, *Lgr6*^{CreER2};*Ctnnb1*$^{f/f}$, *Sox2*^{CreERT2};*Shh*$^{f/f}$, *Sox2*^{CreERT2};*Shh*$^{f/f}$;*Fgfr2b*$^{f/f}$, and *Sox2*^{CreERT2};*Wnt7b*$^{f/f}$ mice 21 days after naphthalene injury.

(B, C, G–I, K, L, and P–R) Relative mRNA expression of *Fgf10*, *Scgb1a1*, *Krt5*, *Tp63*, and*Muc5b* in control, *Gli1*^{CreERT2};*Smo*$^{f/f}$, *Gli1*^{CreERT2}2;*Smo*$^{f/f}$,*Fgf10*$^{f/f}$, *Lgr6*^{CreERT2};*Ctnnb1*$^{f/f}$, *Sox2*^{CreERT2};*Shh*$^{f/f}$, *Sox2*^{CreERT2};*Shh*$^{f/f}$;*Fgfr2b*$^{f/f}$, and *Sox2*^{CreERT2};*Wnt7b*$^{f/f}$ mice 3, 7 and 21 days after naphthalene injury.

(D–F and M–O) (D–F) Quantification of the percent of the airway epithelium covered by club or basal cells in control, *Gli1*^{CreERT2};*Smo*$^{f/f}$, *Gli1*^{CreERT2};*Smo*$^{f/f}$,*Fgf10*$^{f/f}$, *Lgr6*^{CreERT2};*Ctnnb1*$^{f/f}$, *Sox2*^{CreERT2};*Shh*$^{f/f}$, *Sox2*^{CreERT2};*Shh*$^{f/f}$;*Fgfr2b*$^{f/f}$, and *Sox2*^{CreERT2};*Wnt7b*$^{f/f}$ mice.

(S) Schematic representation of data presented in (A) and (J).

**p < 0.01; *p < 0.05. n ≥ 6.; error bars mean ± SEM. Scale bars, 500 μm. Two-sided t test and ANOVA used to determine statistical significance.

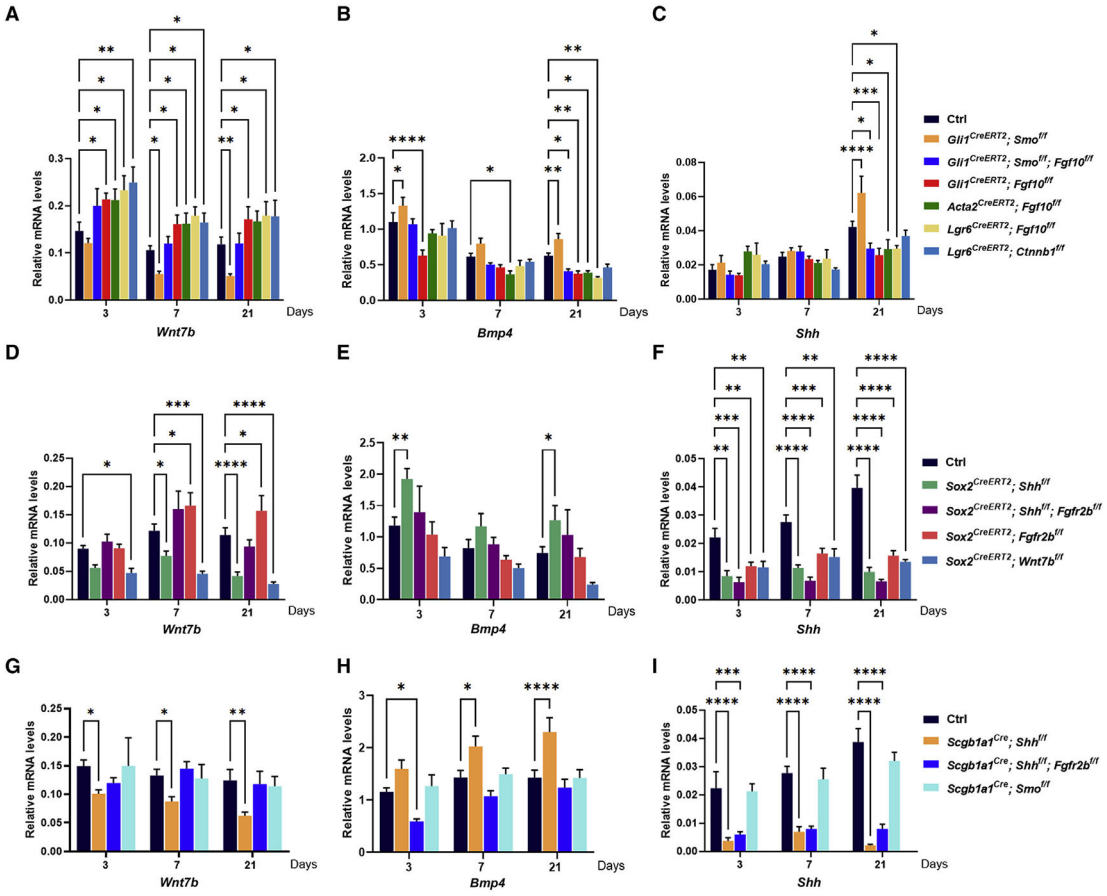

Figure 4. Niche-maintaining cell types communicate with epithelial occupants to fine-tune AESC activation

(A–I) Relative mRNA expression of *Wnt7b*, *Bmp4*, or *Shh* in control, *Gli1*^{CreERT2};*Smo*$^{f/f}$, *Gli1*^{CreERT2};*Smo*$^{f/f}$,*Fgf10*$^{f/f}$, *Gli1*^{CreERT2};*Fgf10*$^{f/f}$, *Acta2*^{CreERT2};*Fgf10*$^{f/f}$, *Lgr6*^{CreERT2};*Fgf10*$^{f/f}$, *Lgr6*^{CreERT2};*Ctnnb1*$^{f/f}$, *Sox2*^{CreERT2};*Shh*$^{f/f}$, *Sox2*^{CreERT2};*Shh*$^{f/f}$;*Fgfr2b*$^{f/f}$, *Sox2*^{CreERT2};*Fgfr2b*$^{f/f}$, *Sox2*^{CreERT2};*Wnt7b*$^{f/f}$, *Scgb1a1*^{Cre};*Shh*$^{f/f}$, *Scgb1a1*^{Cre};*Shh*$^{f/f}$;*Fgfr2b*$^{f/f}$, and *Scgb1a1*^{Cre};*Smo*$^{f/f}$ mice 3, 7, and 21 days after naphthalene injury.

**p < 0.01; *p < 0.05. n ≥ 6.; error bars mean ± SEM. Two-sided t test and ANOVA used to determine statistical significance.

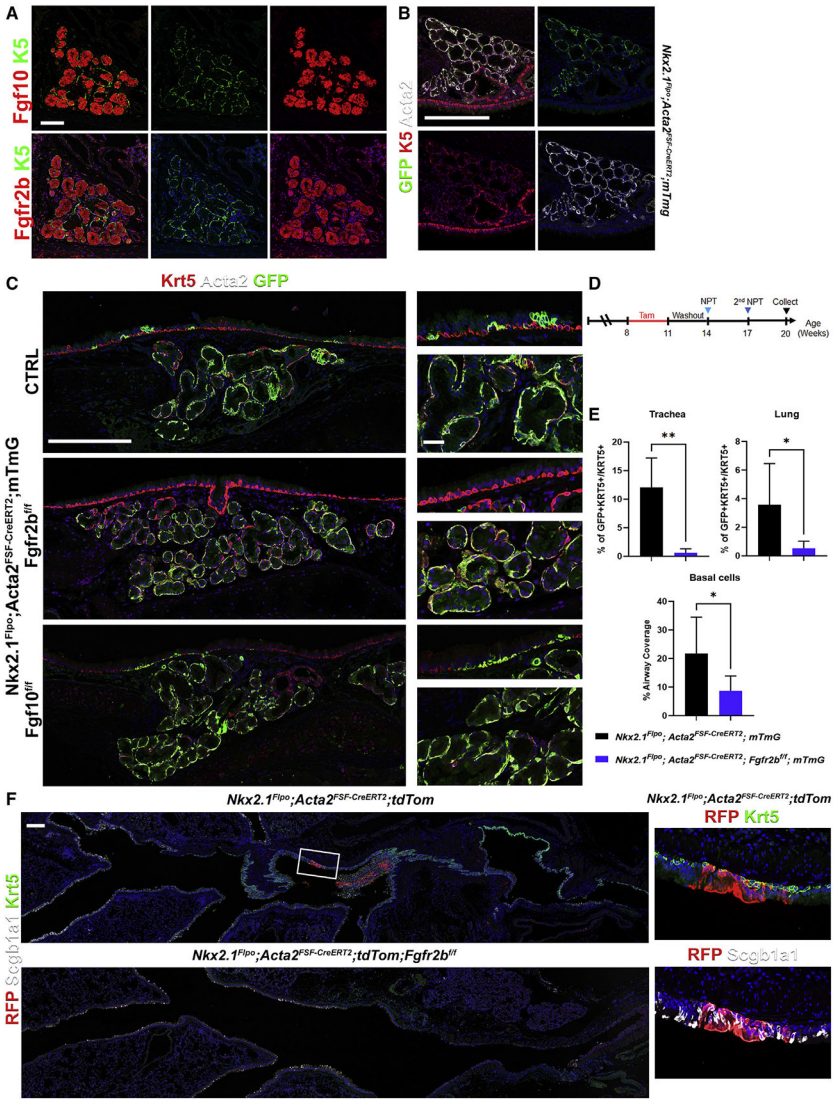

Figure 5. Fgf10 activates different stem cell populations along the proximal distal axis

(A) Immunostaining of human submucosal glands for Fgf10, Fgfr2b, and basal cell marker Krt5 (note the Fgf10 antibody detects Fgf10 bound to receptor).

(B) Immunostaining for GFP and myoepithelial cell markers Krt5 and Acta2 on *Nkx2.1*^{Flpo};*Acta2-Frt-STOP-Frt-Cre*^{ERT2};*Rosa26*^{mTmG} mice.

(C) Immunostaining for GFP and myoepithelial cell markers Krt5 and Acta2 on submucosal glands from *Nkx2.1*^{Flpo};*Acta2-Frt-STOP-Frt-Cre*^{ERT2};*Rosa26*^{mTmG}, *Nkx2.1*^{Flpo};*Acta2-Frt-STOP-Frt-Cre*^{ERT2};*Rosa26*^{mTmG};*Fgfr2b*$^{f/f}$, and *Nkx2.1*^{Flpo};*Acta2-Frt-STOP-Frt-Cre*^{ERT2};Rosa26^{mTmG};*Fgf10*$^{f/f}$ mice that were injured twice with naphthalene with a 21 day interval and were harvested 60 days after the first or 39 days after the second injury. Higher-magnification panels are found to the right.

(D) Schematic representation of experimental design: mice were placed on tamoxifen chow for 3 weeks starting at 8 weeks of age. After a 3 week washout period, mice were i.p. injected with NPT at 14 weeks of age and again 3 weeks later at 17 weeks of age, and lungs were isolated 3 weeks after the second injury at 20 weeks of age.

(E) Top: quantification of the percentage of basal cells that are GFP positive and therefore myoepithelial cell derived in the surface airway epithelium of the tracheas and lungs from *Nkx2.1*^{Flpo};*Acta2-Frt-STOP-Frt-Cre*^{ERT2};*Rosa26*^{mTmG}, *Nkx2.1*^{Flpo};*Acta2-Frt-STOP-Frt-Cre*^{ERT2};*Rosa26*^{mTmG};*Fgfr2b*$^{f/f}$ mice that were injured twice with naphthalene with a 21 day interval and were harvested 60 days after the first or 39 days after the second injury. Bottom: quantification of the percentage of the airway epithelium that is covered by basal cells in *Nkx2.1*^{Flpo};*Acta2-Frt-STOP-Frt-Cre*^{ERT2};*Rosa26*^{mTmG}, *Nkx2.1*^{Flpo};*Acta2-Frt-STOP-Frt-Cre*^{ERT2};*Rosa26*^{mTmG};Fgfr2b $^{f/f}$ mice that were injured twice with naphthalene with a 21 day interval and were harvested 60 days after the first or 39 days after the second injury.

(F) Immunostaining for GFP and club and basal cell markers Scgb1a1 and Krt5, respectively, on lungs from *Nkx2.1*^{Flpo};*Acta2-Frt-STOP-Frt-Cre*^{ERT2};*Rosa26*^{mTmG} and *Nkx2.1*^{Flpo};*Acta2-Frt-STOP-Frt-Cre*^{ERT2};*Rosa26*^{mTmG};*Fgfr2b*$^{f/f}$ mice that were injured twice with naphthalene with a 21 day interval and were harvested 60 days after the first or 39 days after the second injury.

**$p < 0.01$; *$p < 0.05$. $n \geq 6$; error bars mean ± SEM. Scale bars, 200 μm. Two-sided t test and ANOVA used to determine statistical significance.

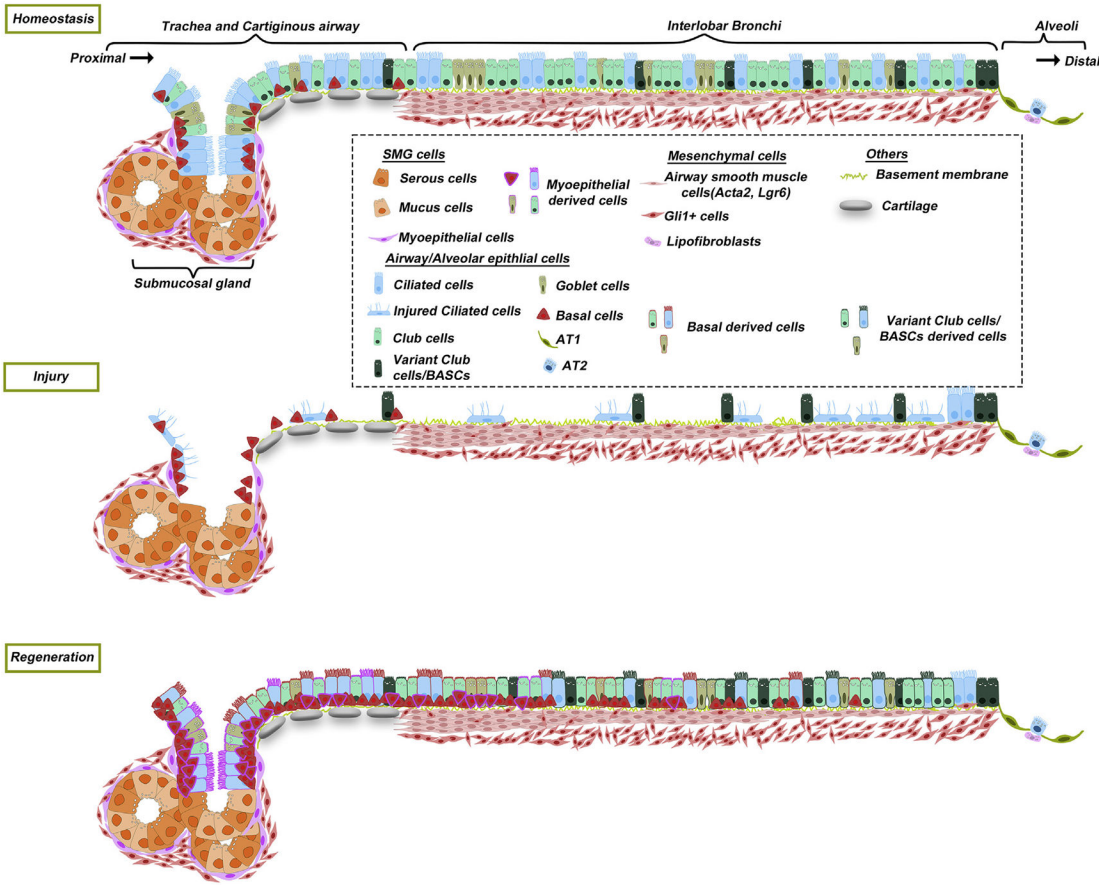

Figure 6. Model of airway epithelial mesenchymal interactions during homeostasis and repair

Here, we show how spatiotemporal expression of Fgf10 by two niche-maintaining cell types is primarily orchestrated by the niche's epithelial occupants—both those that reside prior to and following injury. Prior to injury, differentiated airway epithelial cells secrete Shh to inhibit Fgf10 expression by $Gli1^{+}$ peribronchial mesenchymal cells of the niche. After injury, remaining epithelial cells produce Wnt7b to induce Fgf10 expression in airway smooth muscle cells of the niche. Complete induction of Fgf10 expression in the niche requires loss of an inhibitory Shh signal from the prior epithelial occupant (club cell) as well as induction of an activating Wnt7b signal by the surviving or new epithelial occupant (ciliated and basal cells). We find that this reliance on a common activator of airway epithelial stem cells allows for the recruitment of remote stem cell populations when local populations have been destroyed or exhausted.

KEY RESOURCES TABLE

REAGENT or RESOURCE	SOURCE	IDENTIFIER
Antibodies		
Goat anti-Scgb1a1 (clone T-18)	Santa Cruz Biotechnology Inc.	Cat# sc-9772; RRID: AB_2238819
Rabbit anti-Scgb1a1	Seven Hills Bioreagents	Cat# WRAB-CCSP; RRID: AB_451716
Mouse anti-α-Actin (clone 1A4)	Santa Cruz Biotechnology Inc.	Cat# sc-3251; RRID: AB_262054
Rabbit anti-FGF10	Acris Antibodies	Cat# AP14882PU-N; RRID: AB_1752406
Chicken anti-Green Fluorescent Protein	Aves Labs Inc.	Cat# GFP-1020; RRID: AB_10000240
Rabbit anti-Cytokeratin 5 (clone EP1601Y)	Thermo Fisher Scientific	Cat# MA5-14473; RRID: AB_10979451
Chicken anti-Keratin 5	BioLegend	Cat# 905904; RRID: AB_2721743
Rabbit anti-Mucin 5B (clone H-300)	Santa Cruz Biotechnology Inc.	Cat# sc-20119; RRID: AB_2282256
Rabbit anti-BMP4	Bioss Inc.	Cat# BS-1374R; RRID: AB_10857765
Mouse anti-Shh (clone E–1)	Santa Cruz Biotechnology Inc.	Cat# sc-365112; RRID: AB_10709580
Mouse anti-FoxJ1	Thermo Fisher Scientific	Cat# 14-9965-82; RRID:AB_1548835
Rabbit anti-red fluorescent protein	Rockland Immunochemicals	Cat# 600-401-379; RRID: AB_2209751
Cy3 AffiniPure F(ab')$_2$ Fragment Donkey Anti-Goat IgG (H + L)	Jackson ImmunoResearch	Cat# 705-166-147; RRID: AB_2340413
Cy3 AffiniPure F(ab')$_2$ Fragment Donkey Anti-Mouse IgG (H + L)	Jackson ImmunoResearch	Cat# 715-166-150; RRID: AB_2340816
Cy3 AffiniPure F(ab')$_2$ Fragment Donkey Anti-Rabbit IgG (H + L)	Jackson ImmunoResearch	Cat# 711-166-152; RRID: AB_2313568
Alexa Fluor 647 AffiniPure F(ab')$_2$ Fragment Donkey Anti-Goat IgG (H + L)	Jackson ImmunoResearch	Cat# 705-606-147; RRID: AB_2340438
Alexa Fluor 647 AffiniPure F(ab')$_2$ Fragment Donkey Anti-Mouse IgG (H + L)	Jackson ImmunoResearch	Cat# 715-606-150; RRID: AB_2340865
Alexa Fluor 647 AffiniPure F(ab')$_2$ Fragment Donkey Anti-Rabbit IgG (H + L)	Jackson ImmunoResearch	Cat# 711-606-152; RRID: AB_2340625
Alexa Fluor 488 AffiniPure F(ab')$_2$ Fragment Donkey Anti-Chicken IgY (IgG) (H + L)	Jackson ImmunoResearch	Cat# 703-546-155; RRID: AB_2340376
Alexa Fluor 488 AffiniPure F(ab')$_2$ Fragment Donkey Anti-Goat IgG (H + L)	Jackson ImmunoResearch	Cat# 705-546-147; RRID: AB_2340430
Alexa Fluor 488 AffiniPure F(ab')$_2$ Fragment Donkey Anti-Mouse IgG (H + L)	Jackson ImmunoResearch	Cat# 715-546-150; RRID: AB_2340849
Alexa Fluor 488 AffiniPure F(ab')$_2$ Fragment Donkey Anti-Rabbit IgG (H + L)	Jackson ImmunoResearch	Cat# 711-546-152; RRID: AB_2340619
Chemicals, peptides, and recombinant proteins		
Naphthalene	Sigma-Aldrich	Cat# 84679
Antigen Unmasking Solution, Citrate-Based	Vector Labs	Cat# H-3000
Tamoxifen	Millipore Sigma	Cat# T5648
VECTASHIELD® Antifade Mounting Medium	Vector Labs	Cat# H-1000
Bst LF polymerase	Biolabs Inc.	Cat# M0275L
Proteinase K	Thermo Fisher Scientific	Cat# 25530–049
RNALater	Thermo Fisher Scientific	Cat# AM7021

REAGENT or RESOURCE	SOURCE	IDENTIFIER
Critical commercial assays		
Omega E.Z. RNA Total RNA Kit I	Omega Biotek	Cat #R6834-02
Maxima First Strand cDNA Synthesis	Fisher Scientific	Cat# FERK1642
Taqman Gene Expression Assays	Applied biosystems	Cat# 4369016
Experimental models: Organisms/strains		
Mouse: *Fgfr2b*$^{f/f}$	De Moerlooze et al.	N/A
Mouse: *B6;129S-Sox2*$^{tm1(cre/ERT2)Hoch/J}$ *(Sox2*^{CreERT2}*)*	The Jackson Laboratory	RRID:IMSR_JAX:017593
Mouse: *B6N.129S6(Cg)-Scgb1a1*$^{tm1(cre/ERT)Blh/J}$ *(Scgb1a1*^{CreERT}*)*	The Jackson Laboratory	RRID:IMSR_JAX:01625
Mouse: *Scgb1a1*^{Cre}	Ji et al., Simon and Mariani	N/A
Mouse: *B6.129(Cg)-Gt(ROSA) 26Sor*$^{tm4(ACTB-tdTomato,-EGFP)Luo/J}$ *(Rosa26-mTmG)*	The Jackson Laboratory	RRID:IMSR_JAX:007676
Mouse: *B6.Cg-Gt(ROSA)26Sor*$^{tm9(CAG-tdTomato)Hze/J}$ *(Rosa26-tdTomato)*	The Jackson Laboratory	RRID:IMSR_JAX:007909
Mouse: *Nkx2-1*$^{tm2.1(flpo)Zjh/J}$ *(Nkx2.1*^{flpo}*)*	The Jackson Laboratory	RRID:IMSR_JAX:028577
Mouse: *129S4/SvJae-Fgfr1*$^{tm11.1Sor/J}$ *(Fgfr1*^{Cerulean}*)*	The Jackson Laboratory	RRID:IMSR_JAX:030708
Mouse: *129S4/SvJae-Fgfr2*$^{tm2.1Sor/J}$ *(Fgfr2*^{mCherry}*)*	The Jackson Laboratory	RRID:IMSR_JAX:030710
Mouse: *Krt5*^{CreERT2}	Van Keymeulen et al.	N/A
Mouse: *Acta2*^{CreERT2}	Wendling et al.	N/A
Mouse: *Fgf10*$^{f/f}$	Urness et al.	N/A
Mouse: *B6.129X1-Wnt7b*$^{tm2Amc/J}$ *(Wnt7b*$^{f/f}$*)*	The Jackson Laboratory	RRID:IMSR_JAX:008467
Mouse: B6.129P2-Lgr6tm2.1(cre/ERT)Cle/J (*Lgr6*^{CreERT2}*)*	The Jackson Laboratory	RRID:IMSR_JAX:016934
Mouse: *B6;129-Shh*$^{tm2Amc/J}$ *(Shh*$^{f/f}$*)*	The Jackson Laboratory	RRID:IMSR_JAX:004293
Mouse: *Gli1*$^{tm3(cre/ERT2)Alj/J}$ *(Gli1*^{CreERT2}*)*	The Jackson Laboratory	RRID:IMSR_JAX:007913
Mouse: *Smo*$^{tm2Amc/J}$ *(Smo*$^{f/f}$*)*	The Jackson Laboratory	RRID:IMSR_JAX:004526
Mouse: *Gt(ROSA)26Sor*$^{tm1(Smo/EYFP)Amc/J}$ *(R26SmoM2)*	The Jackson Laboratory	RRID:IMSR_JAX:005130
Mouse: *B6(SJL)-Piezo2*$^{tm1.1(cre)Apat/J}$ *(Piezo2*^{Cre}*)*	The Jackson Laboratory	RRID:IMSR_JAX:027719
Oligonucleotides		
Keratin 5 (*K5*) (qPCR primer)	Thermo Fisher Scientific	Mm01305291_g1
p63 (*Trp63*) (qPCR primer)	Thermo Fisher Scientific	Mm00495788_m1
Scgb1a1 (qPCR primer)	Thermo Fisher Scientific	Mm00442046_m1
Muc5b (qPCR primer)	Thermo Fisher Scientific	Mm00466391_m1
Fgf10 (qPCR primer)	Thermo Fisher Scientific	Mm00433275_m1
Wnt7b (qPCR primer)	Thermo Fisher Scientific	Mm00437358_m1
Bmp4 (qPCR primer)	Thermo Fisher Scientific	Mm00432087_m1
Shh (qPCR primer)	Thermo Fisher Scientific	Mm00436528_m1
β-glucuronidase (qPCR primer)	Thermo Fisher Scientific	Mm00446953_m1
Probes, Branches, Hairpins for SABER-FISH, see Table S1	This paper	N/A
Software and algorithms		
Zen blue	Zeiss	https://www.zeiss.com/
Adobe Photoshop Creative Suite 3	Adobe	https://www.adobe.com/
Graphpad Prism 9.3.1	Graphpad	https://www.graphpad.com/

REAGENT or RESOURCE	SOURCE	IDENTIFIER
LASX	Leica	https://www.leica-microsystems.com/
Other		
Tamoxifen rodent diet (400mg/kg tamoxifen citrate)	Harlan Teklad	Cat# TD.130860